Extracting more information from passive optical tracking observations for reliable orbit element generation

James C. S. Bennett*
SERC Limited, Mount Stromlo Observatory, Cotter Road, Weston Creek, ACT, 2611, Australia
Steven Gehly
SPACE Research Centre, School of Mathematical and Geospatial Sciences, RMIT University, GPO Box 2476, Melbourne, VIC, 3001, Australia

ABSTRACT

This paper presents results from a preliminary method for extracting more orbital information from low rate passive optical tracking data. An improvement in the accuracy of the observation data yields more accurate and reliable orbital elements.

A comparison between the orbit propagations from the orbital element generated using the new data processing method is compared with the one generated from the raw observation data for several objects.

Optical tracking data collected by EOS Space Systems, located on Mount Stromlo, Australia, is fitted to provide a new orbital element. The element accuracy is determined from a comparison between the predicted orbit and subsequent tracking data or reference orbit if available. The new method is shown to result in a better orbit prediction which has important implications in conjunction assessments and the Space Environment Research Centre space object catalogue. The focus is on obtaining reliable orbital solutions from sparse data.

This work forms part of the collaborative effort of the Space Environment Management Cooperative Research Centre which is developing new technologies and strategies to preserve the space environment (`www.serc.org.au`).

Keywords: Orbit determination, tracking, catalogue

1. INTRODUCTION

The Space Environment Research Centre is building capabilities in conjunction assessments and collision warning services. A necessary component of the system is a high accuracy catalogue for the objects of interest.

Optical and laser ranging facilities are being installed in Australia which are dedicated to tracking space debris. Together with EOS Space Systems' Space Debris Tracking Station at Mount Stromlo, Canberra, accurate orbital information will be gathered for a subset of objects to provide conjunction assessments. Initially, conjunction threat warnings will be focussed around partner assets, such as the Optus satellite fleet. As more sensors are installed the catalogue of objects will grow and the conjunction service will be extended.

The Mount Stromlo station is capable of tracking space debris objects using passive optical tracking and/or laser ranging. This paper focusses on the collection of angles-only measurements through the 1.8 metre telescope. The system uses a CCD camera to collect azimuth, β, and elevation, el, measurements.

Measurement error may be introduced by a variety of factors such as atmospheric refraction, sky brightness, system biases and timing errors, mechanical and optical flexure, and so on. A mathematical description of the mechanical

*Email: jamesbennett@serc.org.au

mount is fitted to astrometric observations to map the encoder position to the sky pointing direction. Common mount characteristics are encoder offset error, azimuth/elevation plane non-orthogonality, transverse misalignment, azimuth axis misalignments, tube flexure, etc. The success of the mount modelling process is dependent on the repeatability of the error. For more information consult [10]. Typically, a mount model fit results in around 1–3 arc-seconds root mean square (RMS) pointing accuracy.

The optical tracking system generates an optical track, $O_i = \{(t_i, \beta_i, el_i)\}$, where t_i is the epoch of the observation (receive time of light detection on the focal plane), and β_i, el_i are the azimuth and elevation at the observation epoch, respectively. The rate of collection is restricted by the camera exposure time which may be lengthened for fainter objects, which reduces the observation generation rate. Four more quantities are needed to form a 6-dimensional state vector. Towards quantifying the 6d state, the angular observations are fitted using a least squares Chebyshev polynomial fitting procedure and smoothed observations are generated, with the rate of change also determined. During the process, astrometric data is fused with the observations and the result is 4d observational data $(\beta, \dot{\beta}, el, \dot{el})$ rather then the original 2d azimuth and elevation observations. The subsequent 4d observation set leaves 2 quantities $(\rho, \dot{\rho})$ to determine an orbital state vector. One can form an *admissible region* to place bounds on the $(\rho, \dot{\rho})$ space and sample to construct a set of discrete hypothesis state vectors. The number of possible state vectors is reduced through data association methods in the attempt to identify a unique solution [3].

This paper focusses on a method to create azimuth and elevation rates from the angular tracking data. The utility of the 4d data in defining admissible regions is briefly discussed as methods will be developed in SERC for multi-target and event detection and correlation during a planned GEO tracking campaign for conjunction threat warnings.

2. METHODS

Fitting optical observations to generate angular rate information is not a new concept. DeMars et al. [3] computed the angular rate information by fitting high rate 500 Hz raw angular data, simulated to be descriptive of measurements from a photon counter [2], using a linear least squares fit. They provide a comparison between an angles only initial orbit determination (IOD) scheme and one where the angular rates were also used using admissible regions and a multiple hypothesis filtering approach. It is shown that the IOD considering the rates is more accurate and reliable than the angles only case.

The observation data rate for the processing in this paper is much lower at ≈ 2 Hz. If there are outliers present in the data then a fitted observation may be corrupted. Chebyshev polynomial fitting is chosen to overcome ill-conditioning.

2.1. Sampling of azimuth and elevation observations using Chebyshev polynomial fitting

Chebyshev polynomials are used in many applications of numerical analysis [6]. They are a set of orthogonal polynomials and can be defined recursively. In this section, Chebyshev polynomial fitting is used to determine fitted points and rates of change for an angles-only track.

The Chebyshev polynomials $T_n(x)$ of the first kind may be expressed recursively [1]:

$$T_0(x) = 1, \tag{1}$$

$$T_1(x) = x, \tag{2}$$

$$T_{n+1}(x) = 2xT_n(x) - T_{n-1}(x), \quad n \geq 1. \tag{3}$$

The approximating function, $f(x)$, may be determined as:

$$f(x) = \sum_{n=0}^{\infty} a_n T_n(x), \quad x \in [-1, 1], \tag{4}$$

once the coefficients a_i have been found.

The gradient of the Chebyshev polynomials of the first kind may be expressed in terms of the Chebyshev polynomials of the second kind through the relationship:

$$\frac{d}{dx}T_n(x) = nU_{n-1}(x), \quad n \geq 1, \tag{5}$$

where the Chebyshev polynomials of the second kind are:

$$\begin{aligned} U_0(x) &= 1, & (6)\\ U_1(x) &= 2x, & (7)\\ U_{n+1} &= 2xU_n(x) - U_{n-1}(x), \quad n \geq 1. & (8) \end{aligned}$$

Then, the gradient of the approximating function, $f'(x)$, is given by:

$$f'(x) = \sum_{n=1}^{\infty} a_n n U_{n-1}(x). \tag{9}$$

In what follows, the azimuth and elevation observation data is fitted using piecewise quadratic Chebyshev polynomials:

$$f_\beta(x) = \sum_{n=0}^{2} a_n T_n(x), \quad f_{el}(x) = \sum_{m=0}^{2} a_m T_m(x), \quad x \in [-1, 1], \tag{10}$$

where $f_\beta(x), f_{el}(x)$ are the fit functions for azimuth and elevation, respectively. The time interval of the fit, $t \in [t_a, t_b]$ is mapped to $x \in [-1, 1]$ with the transformation $x = (2t - (t_a + t_b))/(t_b - t_a)$.

The azimuth residual, r_{β_i}, is calculated as:

$$r_{\beta_i} = \beta_i - f_\beta(x_i), \tag{11}$$

and the parameters may be determined by minimising the standard least squares cost function:

$$J = \sum_{i=1}^{N} r_{\beta_i}^2, \tag{12}$$

where N is the number of observations. The parameters may then be determined from:

$$\mathbf{X}_\beta = (A^T A)^{-1} A^T \mathbf{b}, \tag{13}$$

where $A = \frac{\partial r_{\beta_i}}{\partial \mathbf{X}_\beta}$, $\mathbf{X}_\beta = [a_0 \quad a_1 \quad a_2]^T$, and $\mathbf{b}$ is the observation vector. These steps are then repeated for the elevation. Once the fitted functions are determined, the observation at the epoch of interest and the rate of change are determined. If the RMS of the fit is more than 5 arc-seconds then the sampled point is rejected.

A quadratic fit function was chosen so that the analysis can be readily extended to include angular acceleration estimates although the current analysis is limited to the generation of angular rates. Once the angular acceleration terms are approximated then they may be used to solve for the range and range rate from the equations of motion. However, these may only suffice as estimates of the range and range rate due to having large uncertainties [5]. This will be considered in future studies and will be tested using the current method.

2.2. Fitted observation error determination

To determine the accuracy of the generated sampled angles and their rates, accurate International Laser Ranging Service (ILRS) Consolidated Prediction Format [8] (CPF) data is used as the reference. The CPF reference orbit is in a True Earth-Centred Earth-Fixed (ECEF) coordinate system.

The geocentric position and velocity vectors of the CPF reference orbit are denoted as $\mathbf{r}_{ECEF}$, and $\mathbf{v}_{ECEF}$, respectively, and are related to the slant range vector from the site to the satellite by:

$$\mathbf{r}_{ECEF} = \mathbf{r}_{site} + \boldsymbol{\rho}_{ECEF}, \tag{14}$$

$$\mathbf{v}_{ECEF} = \dot{\boldsymbol{\rho}}_{ECEF}, \tag{15}$$

where $\mathbf{r}_{site}$ is the invariant point of the telescope in True ECEF, and $\boldsymbol{\rho}_{ECEF}$ is the range vector from the site to the satellite, also in True ECEF.

The topocentric slant range vector is given by:

$$\boldsymbol{\rho} \equiv \boldsymbol{\rho}_{NEU} = \begin{bmatrix} \rho_N \\ \rho_E \\ \rho_U \end{bmatrix} = \begin{bmatrix} \rho^* \cos(el^*) \cos(\beta^*) \\ \rho^* \cos(el^*) \sin(\beta^*) \\ \rho^* \sin(el^*) \end{bmatrix}, \tag{16}$$

where $\boldsymbol{\rho}_{NEU}$ is in the North-East-Up (NEU) system, a "*" is used to denote the quantities as truth, and ρ^*, β^*, and el^* are the range, azimuth, and elevation from the site to the reference CPF orbit.

The transformations between ECEF and NEU for the slant range vector and velocity are:

$$\boldsymbol{\rho}_{ECEF} = \begin{bmatrix} -\cos(\lambda)\sin(\phi) & -\sin(\lambda) & \cos(\lambda)\cos(\phi) \\ -\sin(\lambda)\sin(\phi) & \cos(\lambda) & \sin(\lambda)\cos(\phi) \\ \cos(\phi) & 0 & \sin(\phi) \end{bmatrix} \begin{bmatrix} \rho_N \\ \rho_E \\ \rho_U \end{bmatrix}, \tag{17}$$

$$\dot{\boldsymbol{\rho}}_{ECEF} = \begin{bmatrix} -\cos(\lambda)\sin(\phi) & -\sin(\lambda) & \cos(\lambda)\cos(\phi) \\ -\sin(\lambda)\sin(\phi) & \cos(\lambda) & \sin(\lambda)\cos(\phi) \\ \cos(\phi) & 0 & \sin(\phi) \end{bmatrix} \begin{bmatrix} \dot{\rho}_N \\ \dot{\rho}_E \\ \dot{\rho}_U \end{bmatrix}. \tag{18}$$

Eqs. (14) – (18) can then be used to calculate $(\beta^*, \dot{\beta}^*, el^*, \dot{el}^*, \rho^*, \dot{\rho}^*)$ from the known site location. The azimuth and elevation angles are then given by:

$$el^* = \arcsin(\rho_U/\rho^*), \quad az^* = \arctan2(\rho_E, \rho_N). \tag{19}$$

The range, elevation, and azimuth rates are:

$$\dot{\rho^*} = \frac{\boldsymbol{\rho} \cdot \dot{\boldsymbol{\rho}}}{\rho^*}, \quad \dot{el}^* = \frac{\dot{\rho}_U - \dot{\rho^*}\sin(el^*)}{\sqrt{\rho_N^2 + \rho_E^2}}, \quad \dot{\beta}^* = \frac{\dot{\rho}_E\rho_N - \dot{\rho}_N\rho_E}{\rho_N^2 + \rho_E^2}. \tag{20}$$

See [11] for more information on the transformations used in this section. Once $(\beta^*, \dot{\beta}^*, el^*, \dot{el}^*)$ have been determined the residuals of the observations are calculated.

2.3. Orbit determination

A least-squares estimation procedure was employed to test the resulting orbit prediction accuracy from an orbit estimated from the original observations compared with one estimated from the fitted/corrected observations. The latest two line element (TLE) before the OD start epoch was downloaded from `www.space-track.org` and used as the initial state. The force model comprised a 70 degree and order EGM96 gravity model, solar radiation pressure effects with Earth shadowing, Solar-Lunar and planetary gravity, Earth albedo, general relativity, and Earth tides.

Results are presented for orbit predictions for Lageos 1 and Lageos 2 as well as three non-spherical objects.

3. RESULTS

In this section, the accuracy of the Chebyshev polynomial fitting is determined for the fitted azimuth and elevation and their rates. Then these observations are fitted in the OD study and the results comparing the orbital solutions are presented. Where reference data is not available, i.e. for all objects other than Lageos 1 and Lageos 2, the errors are determined as the RMS difference between the computed orbit prediction and the observational data in 2d.

3.1. Fitted observation error

The accuracy of the method described in the previous section is determined for the Lageos 1 and Lageos 2 satellite observations collected during February to July, 2016. A total of 26 passes were analysed and the residuals calculated by comparing to accurate CPFs[1] as described in the previous section. Fig. 1 shows the residuals of the sampled observations and their calculated rates. The RMS error for the sampled azimuth and elevation is 0.9 arc-seconds. The

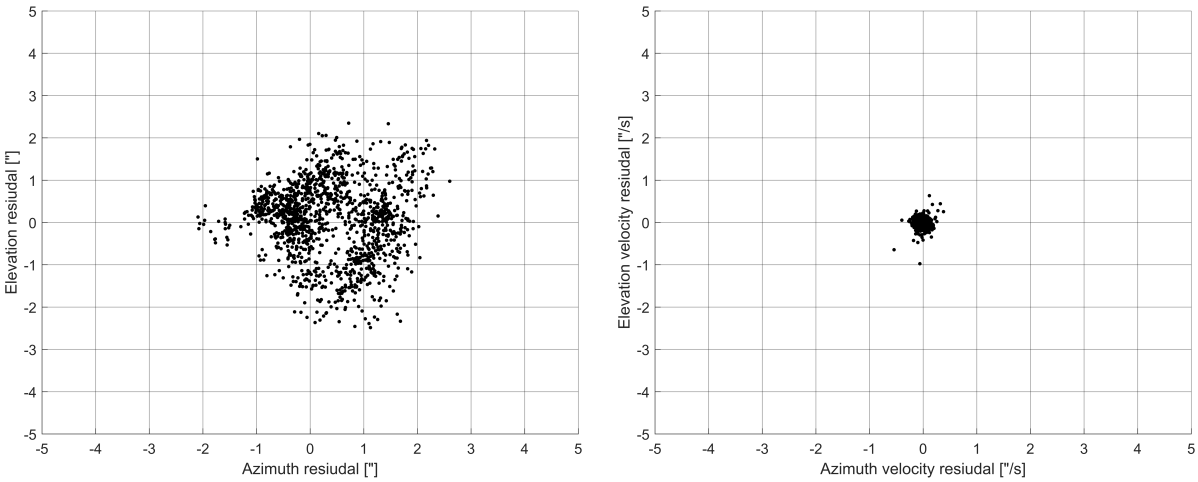

(a) Angular error: $\sigma_\beta = 0.9, \quad \sigma_{el} = 0.9$

(b) Angular velocity error: $\sigma_{\dot{\beta}} = 0.07, \quad \sigma_{\dot{el}} = 0.09$

Fig. 1. Observation residuals for Lageos 1 and 2

RMS error for the azimuth and elevation rates is 0.07 and 0.09 arc-seconds per second, respectively. Fitting the data with Chebyshev polynomials was found to be much more reliable and accurate than regular polynomial fitting due to avoiding ill-conditioning.

3.2. Orbit prediction results

A comparison between an orbit determined by fitting the original full rate observations with one determined by fitting the sampled observations for Lageos 1 and Lageos 2 is presented first. The orbit determined in each case was then propagated and compared with the CPF reference orbit and the Euclidean distance was calculated. In the fitting process, only the sampled azimuth and elevation observations were fitted, i.e. the angular rate observations were neglected. The orbit determination conditions are shown in Tab. 1.

Tab. 1. Orbit determination conditions for Lageos 1 and 2

Satellite	NORAD ID	Perigee [km]	Apogee [km]	Initial Epoch [year=2016]	OD Span [days]	# Obs Full	# Obs Sampled	# Passes
Lageos 1	8820	5,838	5,948	17-Feb 00:00 UTC	3	1226	44	3
Lageos 2	22195	5,616	5,949	17-Feb 00:00 UTC	9	980	37	5

Fig. 2 shows a comparison between the orbit prediction from fitting the full rate observations and one fitting the sampled angles for Lageos 1 and Lageos 2. In each case presented, the fitted observations yield a better orbit prediction. The orbit determination process for the sampled observations case is also computationally faster due to the reduction in the number of observations to process. In the Lageos 1 case, outliers in the original observations have corrupted the orbital solution. These were removed by the correction and fitting method.

[1] `ftp://cddis.gsfc.nasa.gov/slr/cpf_predicts/`, accessed July 2016.

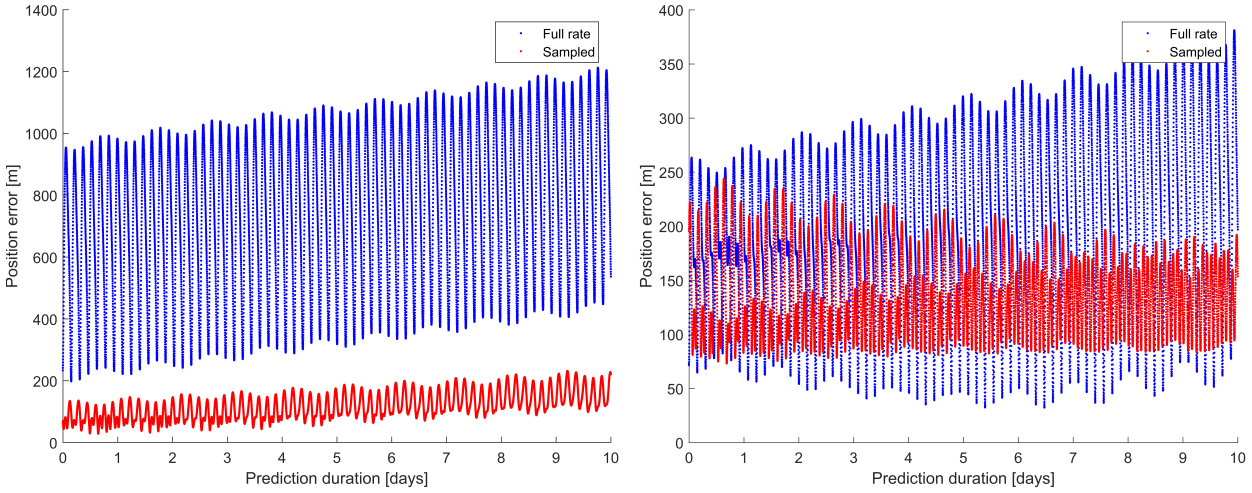

(a) Lageos 1 (b) Lageos 2

Fig. 2. Orbit prediction comparisons for Lageos 1 and 2

Next, the non-spherical objects are considered. The conditions for the ODs for the non-spherical cases presented are contained in Tab. 2. The orbit prediction errors for NAVSTAR 48 and NAVSTAR 71 are shown in Fig. 3. Fig. 4 shows

Tab. 2. Orbit determination conditions

Satellite	NORAD ID	Perigee [km]	Apogee [km]	Initial Epoch [year=2016]	OD Span [days]	# Obs [Full]	# Obs [Sampled]	# passes
NAVSTAR 48 (USA 151)	26407	19,648	20,715	21-Feb 00:00 UTC	5	1022	38	4
NAVSTAR 71 (USA 256)	40105	20,175	20,192	19-Feb 00:00 UTC	7	1975	105	5
GORIZONT 1	11158	21,303	50,275	21-Feb 00:00 UTC	5	859	54	4

the orbit prediction results for the debris object GORIZONT 1. In all of the cases considered the sampled observations result in better orbit predictions. The post-processing method has been implemented and corrected observations are routinely produced.

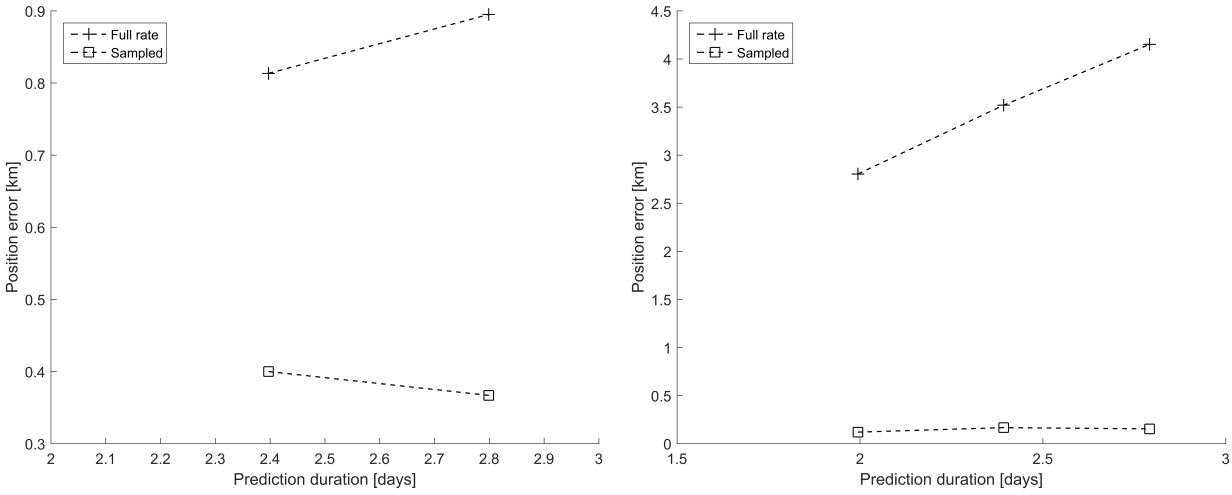

(a) NAVSTAR 48 (USA 151)

(b) NAVSTAR 71 (USA 256)

Fig. 3. Orbit prediction comparisons for for NAVSTAR 48 and NAVSTAR 71

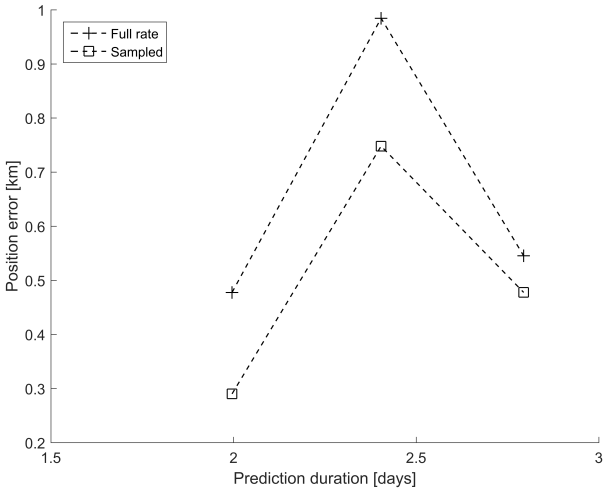

Fig. 4. Orbit prediction comparisons for GORIZONT 1

4. DISCUSSION

This paper presented a method for deriving angular rates from the azimuth and elevation observations using Chebyshev polynomial fitting. To improve accuracy, effort will be placed on refining the method to better identify outliers and improve the throughput of the sampled observation generation. A higher observation generation rate is expected to improve the results and further improvements may be gained by equipping the system a photon counter, at the possible expense of data corruption if the object is not kept on the boresight, i.e. light from stars may be present in the photon returns.

Initial orbit determination using admissible regions has been investigated extensively in the literature, see [3, 4, 5, 7, 9] and references therein. With the inclusion of the angular rates, the search region is reduced to 2 dimensions. When laser ranging, the range information currently provides one more dimension of information. The method presented in this paper will be applied to the range data in a future paper, thus giving full state information $(\beta, \dot{\beta}, el, \dot{el}, \rho, \dot{\rho})$ for each fitted observation. Together with the estimates for the angular accelerations, methods will be explored for multiple object identification and association in a wide field of view optical telescope as well as event detection.

The orbit determination code will be extended to process angular and range rates. This is expected to improve the orbit determinations, particularly in sparse data scenarios.

In the last quarter of 2016 a new optical and laser tracking site will be commissioned in Western Australia. This site is a joint effort between EOS Space Systems and Lockheed Martin. This station has a baseline separation of more than 3,500 km from Mount Stromlo and will have several tracking telescopes for LEO-to-GEO active and passive tracking. This will improve the reliability of the orbit determinations due to improved geometry.

ACKNOWLEDGEMENTS

The authors would like to acknowledge the support of the Cooperative Research Centre for Space Environment Management (SERC Limited) through the Australian Governments Cooperative Research Centre Programme. The authors would also like to acknowledge Dr Michael Lachut (SERC), Dr Craig Smith (EOS Space Systems), and Dr Ben Greene (SERC) for their useful feedback on the manuscript.

REFERENCES

[1] Abramowitz, M. and I.A. Stegun, Handbook of Mathematical Functions with Formulas, Graphs, and Mathematical Tables. Applied Mathematics Series. 55 (tenth printing, December 1972, with corrections). 1972.

[2] Bloch, J. and R. Rast, Space Surveillance One Photon at a Time, in *Advanced Maui Optical and Space Surveillance Technologies Conference*, Maui, Hawaii, September 12-15, 2007.

[3] DeMars, K.J., M.K. Jah, and P.W. Schumacher, Initial Orbit Determination using Short-Arc Angle and Angle Rate Data, *IEEE Transactions on Aerospace and Electronic Systems*, 48(3): p. 2628-2637, 2012.

[4] Fujimoto, K. and K.T. Alfriend, Optical Short-Arc Association Hypothesis Gating via Angle-Rate Information, *Journal of Guidance, Control, and Dynamics*, 38(9): p. 1602-1613, 2015.

[5] Maruskin, J.M., D.J. Scheeres, and K.T. Alfriend, Correlation of Optical Observations of Objects in Earth Orbit. *Journal of Guidance, Control, and Dynamics*, 32(1): p. 194-209, 2009.

[6] Mason, J.C. and D.C. Handscomb, *Chebyshev Polynomials*, Chapman & Hall / CRC, 2003.

[7] Milani, A., Tommei, G., Farnocchia, D., Rossi, A., Schildknecht, T., and Jehn, R., Correlation and orbit determination of space objects based on sparse optical data, *Monthly Notices of the Royal Astronomical Society*, 417(3): p. 2094-2103, 2011.

[8] Ricklefs, R.L., Consolidated Laser Ranging Prediction Format, Version 1.01. 2006, `http://ilrs.gsfc.nasa.gov/docs/2006/cpf_1.01.pdf`.

[9] Tommei, G., A. Milani and A. Rossi, Orbit determination of space debris: admissible regions, *Celestial Mechanics and Dynamical Astronomy*, 97: 289-304, 2007.

[10] Trueblood, M. and R. Genet, *Telescope Control*, Willmann-Bell, Incorporated, 1997.

[11] Vallado, D.A., *Fundamentals of Astrodynamics and Applications*. Fourth ed.: Microcosm Press, Hawthorne, CA, 2013.